This is a preprint of a paper that appeared in the Proceedings of the IEEE RAS/EMBS International Conference on Biomedical Robotics and Biomechatronics (BioRob), 2012, Rome

Conception and Evaluation of a Novel Variable Torsion Stiffness for Biomechanical Applications

J. Schuy, P. Beckerle, *Member, IEEE*, J. Wojtusch, S. Rinderknecht, and O. von Stryk, *Member, IEEE*

***Abstract*— This paper proposes a novel variable torsion stiffness (VTS) aiming on biomechanical applications like prosthetic knee joints. By varying the effective length of a torsional elastic element via a relocatable counter bearing, the stiffness of a rotational joint is adjusted. This functional concept is described in detail by the authors as well as the design of such VTS joints. Additionally, analytical models for the transfer behaviour of drivetrain and stiffness control are derived. These are used for a simulative evaluation of a pendulum driven by a VTS unit. Based on the results of this simulation, the power requirements of VTS are analysed. Furthermore, an analysis of its structural strength is presented. For practical comprehensibility, the example of the design of a prosthetic knee joint is taken up for several times in this paper. Finally, the concept, modeling and design of VTS as well as the simulation results are concluded and discussed in a final assessment and in comparison to other contemporary concepts.**

I. INTRODUCTION

In industrial robots, requirements for actuators are high dynamics, precision in position control, high holding torques and hence high joint stiffness. Due to closer human-machine-interactions, stiff robotic joints in combination with physical proximity increase the risk of harming humans by collision - e.g., in humanoid robots and service robots. Thus, there is a need for series elastic actuator concepts, which modify their stiffness depending on the situation. This can be high stiffness for precision and dynamics as well as high compliance for safety and energy absorption. Such concepts also enable to absorb shock loads, protect the mechanical setup from destructive peak torques and perform smooth movements. Further objectives can be the increase of energy efficiency by energy storage in the elastic element, especially in the case of oscillating motion, or the reduction of vibrations. As shown in [1]–[3] the efficiency can be improved by matching the natural frequency of a series elastic actuator to the frequency of the desired trajectory. A possible application of such joints are biomechanical devices like ortheses, prostheses or exoskeletons. Since the stiffness of biomechanical joints varies during movement, a technical counterpart is required to adapt its stiffness comparable and thus independently from the joint position.

This work was funded by Forum for Interdisciplinary Research of Technische Universität Darmstadt.

J. Schuy, P. Beckerle, and S. Rinderknecht are with Department of Mechanical Engineering, Institute for Mechatronic Systems in Mechanical Engineering, Technische Universität Darmstadt, 64287 Darmstadt, Germany. schuy | beckerle | rinderknecht@ims.tu-darmstadt.de

J. Wojtusch and O. von Stryk are with Department of Computer Science, Simulation, Systems Optimization and Robotics Group, Technische Universität Darmstadt, 64289 Darmstadt, Germany. wojtusch | stryk@sim.tu-darmstadt.de

In the middle of the 1990s, first concepts of actuators with variable stiffness like the Series Elastic Actuator (SEA) [1], [4] as well as the Mechanical Impedance Adjuster (MIA) [5] have been presented. While the force-controlled SEA is based on a fixed-stiffness spring in series with a stiff actuator, MIA adjusts the stiffness via the active length of a leaf spring. In 2009, Van Ham et al. categorizes the fundamental principles of generating variable compliances into four groups: Equilibrium-controlled, antagonistic-controlled, structure-controlled and mechanically controlled stiffness [6]. While the equilibrium-controlled principle changes the equilibrium position of a spring to generate a desired force or stiffness [7], the antagonistic-controlled principle is based on two or more actuators with non-adaptable stiffness, coupled antagonistically and working against each other similar to human muscles. Structure-controlled compliant actuators change the stiffness due to a modification of the physical structure of an elastic element - e.g., the moment of inertia or the effective elastic length. In contrast to this, mechanically controlled compliant actuators always use the full length of the elastic element and adjust the stiffness by pretension. Most of the present concepts can be sorted into this classification. The SEA belongs to the group of the equilibrium-controlled principle, while the concepts of MIA, VSJ [8], JackSpring™ [9] represent structure-controlled approaches. Examples for mechanically controlled concepts are MACCEPA [10], VSA [11], [12], VS-Joint [13], HDAU [14], AwAS [15], [16], MARIONET [17], rHEA [18], the concept from [19] and pleated artificial muscles [20]. The latter concept is usually implemented in antagonistic setups and hence classified to the antagonistic-controlled principle. Concepts for antagonistic-controlled stiffness are AMASC [21], PDAU [14], VSSEA [22] and the one presented in [23]. Quasi-antagonistic approaches as QAJ [24] and ANELS [25] consist of a direct drive in combination with an antagonistic stiffness variation unit. Beyond this categorization, there are concepts like SDAU [14] with a direct drive in combination with a deceleration actuator or VSU [26] based on a stiffness modification by magnetic forces.

The Variable Torsion Stiffness (VTS) presented in this paper is based on the principle of structure-controlled stiffness variation. Aiming on applications in biomechanically inspired robotic joints, the torsional stiffness of a rotational setup is adjusted by varying the effective length of an elastic element. In contrast to the translational elements used in most other contemporary approaches, the obtained design provides a large bandwidth of stiffness, high dynamics and high torque

in a compact and customizable actuator. The functional concept of VTS is explained in Section II. Analytical models of the drivetrain and the compliance control are derived in Section III. Subsequently, Section IV gives insights into the functional design, while Section V presents a simulative evaluation of VTS. Finally in Section VI, a conclusion and brief discussion of the results including a comparison to [27] as well as an outlook on further works are given.

II. FUNCTIONAL CONCEPT

In this section the conceptional background of the proposed variable torsion stiffness is presented. Its functionality is based on the principle of structure-controlled elasticity [6] and depicted in the sketch in Figure 1. The system consists of two actuators and an elastic element realizing the compliant part. Actuator 1 applies a torque τ_i to the elastic element - e.g., a cylinder with torsional elasticity - which is used for propulsion of the moved link. Independently from this movement, actuator 2 is used to adjust the system's stiffness by varying the location of a counter bearing on the elastic element. Hence, the input torque τ_i is transformed to the output torque τ_o via the variable compliant part.

The torsional stiffness of a cylinder can be described as

$$k_{vts}(x) = \frac{G\,I_t(x)}{x} \tag{1}$$

based on the principles of elastostatics [28]. This stiffness depends on the used material's modulus of elasticity in shear G, the torsional moment of inertia $I_t(x)$ and the active length x of the elastic element. This active length x is determined by the distance between the bearing fixed to the position of actuator 1 and the adjustable counter bearing on the elastic element. Assuming a thick-walled hollow cylinder as the elastic element, its torsional moment of inertia $I_t(x)$ can be modified by varying its geometry by means of its inner radius $r(x)$ and outer radius $R(x)$ [28]. To simplify the geometric design, both parameters $r(x)$ and $R(x)$ are specified to be constant over the functional length l and coupled by a constant factor $\lambda = \frac{r}{R}$. Thus, the torsional moment of inertia $I_t(x)$ is determined by

$$I_t = \frac{\pi(R^4 - r^4)}{2} = \frac{\pi}{2}(1-\lambda^4)R^4\ . \tag{2}$$

Since the shear modulus G is a material property, it is determined by choosing a material. With this set of variable parameters, a customized basic stiffness could be set by its selection.

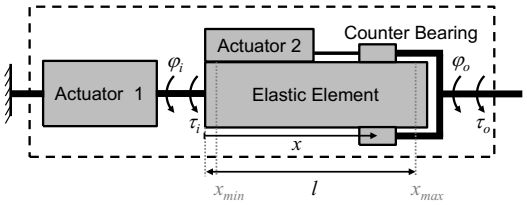

Fig. 1. Sketch of the principle VTS functionality.

III. ANALYTICAL MODELLING

The concept of the variable torsion stiffness can be classified as a structure-controlled variable compliant actuator [6]. Its behaviour can be distinguished into two different paths. These paths will both be modeled analytically in this section and couplings between the paths will be shown. First, a derivation of a model for the transfer behaviour of the compliant drivetrain will be described. Subsequently, a model for stiffness control path, which varies the stiffness of the drivetrain and is driven by the second actuator, will be given.

A. Drivetrain Transfer Behaviour

Since the variable torsion stiffness represents a mechanical transformer with variable characteristics, it can be described by its transfer behaviour between drivetrain input and output. On the input side, actuator 1 applies the input torque τ_i leading to an angular position φ_i. On the output side, a torque τ_o and a resulting angular position φ_o are induced by this. For the characterisation of the torsional effects, the torsional angle $\vartheta = \varphi_o - \varphi_i$ and the inner torque of the elastic element $\tau_t = \tau_o - \tau_i$ are considered.

The kinematics of an infinitesimal part of the system can be modeled by $r\,d\vartheta = \gamma\,dx$ in case of small torsional angles ϑ [28]. Here, $d\vartheta$ represents the radial torsional angle and γ the shear strain of the infinitesimal element. Combining this relation with the law of elasticity $\sigma_s = G\gamma$ and assuming a constant I_t, leads to an ordinary differential equation for the torsional behaviour of the element under the shear stress σ_s that is induced by the inner moment τ_t, which is $G\,I_t\,\vartheta' = \tau_t$.

In order to calculate the value of ϑ at the end of the active part of the elastic element (ϑ_x), this equation is rearranged to $\vartheta' = \frac{\tau_t}{G I_t}$ and integrated over the active length x, leading to

$$\vartheta_x = \frac{\tau_t\,x}{G\,I_t}. \tag{3}$$

With (3), the inner torque τ_t of the elastic element can be described as

$$\tau_t = \frac{G\,I_t}{x}\vartheta_x = k_{vts}(x)\,\vartheta_x \tag{4}$$

and its torsional stiffness can be determined. Hence, the stiffness k_{vts} of this element corresponds to the one given in (1) and a model of the drivetrain's transfer behaviour can be given as $\tau_o - \tau_i = k_{vts}(x)(\varphi_o - \varphi_i)$.

B. Stiffness Control Model

Modeling the stiffness control path is important for analyzing the energy consumption of the system especially, since moving the counter bearing on the elastic element leads to energy dissipation by friction. Thus, the counter bearing can be modeled by a block moving on a surface with a coefficient of friction μ. This block receives a normal force F_n that induces a coulomb-type frictional force

$$F_f = \mu\,F_n \tag{5}$$

acting against its direction of motion. This block always moves on a plain surface, since the slope of the elastic element's torsional displacement is always zero at the position x of the counter bearing. The kinematics of the system are depicted in Figure 2.

Since the normal force F_n is induced by the inner torque τ_t of the elastic element and the mean radial distance of the counter bearing r_n, it can be determined by the drivetrains transfer behaviour as

$$F_n = -\frac{\tau_t}{r_n} = -\frac{k_{vts}(x)}{r_n}\vartheta_x \ . \tag{6}$$

Inserting this relationship into (5) leads to a model of the frictional effects in the counter bearing that are working against the stiffness control by actuator 2, that is

$$F_f = -\mu\,\frac{k_{vts}(x)}{r_n}\vartheta_x \ . \tag{7}$$

Assuming an ideal actuator, this force is the only one that has to be overcome in order to move the counter bearing. Hence, only these frictional effects are considered for a first assumption of the energy consumption. Additionally, these effects only appear, if the counter bearing is moved while the elastic element shows a torsional displacement $\vartheta \neq 0$.

IV. FUNCTIONAL DESIGN

In order to determine the geometric design of the elastic element, the required stiffness characteristics have to be considered as well as the basic conditions given by the specific application. While the stiffness characteristics are mainly determined by the inner radius r and outer radius R of the element, its functional length l also depends on the available installation space. For the purpose of finding geometric parameters corresponding to the required stiffness characteristics, it is recommendable to link up the inner radius r and the outer radius R by the constant factor λ given in (2). Hence, by inserting (2) into (1), the stiffness k_{vts} is given as a function of the outer radius R

$$k_{vts} = \frac{\pi\,G(1-\lambda^4)R^4}{2x} \tag{8}$$

with $x_{min} \geq x \geq x_{max}$. This allows to choose the factor λ according to previously specified stiffness requirements, which might be given as a maximum stiffness $k_{vts,max}$ at an minimum active length x_{min} for example. Thus, the latter

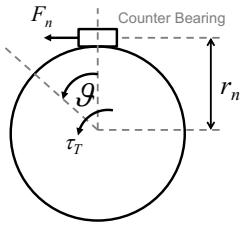

Fig. 2. Sketch of the stiffness control path.

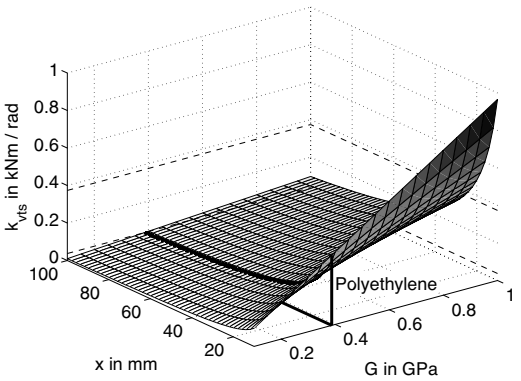

Fig. 3. General stiffness k_{vts} (shaded mesh) and specific stiffness $k_{vts,PE}$ for polyethylene (black line) with a desired stiffness range (dashed line) versus active length x and shear modulus G.

values are inserted into (8) and it is reanranged to give the outer radius R depending on λ

$$R = \sqrt[4]{\frac{2\,k_{vts,max}\ x_{min}}{\pi\,G(1-\lambda^4)}} \ . \tag{9}$$

With this equation, it is possible to specify λ in a way that leads to a geometry suiting the practical application, which might be a maximum outer radius R and the shear modulus G of an existing material.

For the example of a prosthetic knee, the functional length might have a value of $l = 100\,\mathrm{mm}$ and the outer radius might be limited to $R = 10\,\mathrm{mm}$. According to [3] a stiffness ranges from about $50\,\frac{\mathrm{Nm}}{\mathrm{rad}}$ to $350\,\frac{\mathrm{Nm}}{\mathrm{rad}}$ is aimed. With these requirements for the geometry and the stiffness k_{vts}, the material, the outer radius R and the factor λ can be chosen iteratively. Figure 3 shows the characteristics of the stiffness for an outer radius $R = 9\,\mathrm{mm}$ and $\lambda = 0.5$ versus active length x and shear modulus G. Based on the required stiffness range, polyethylene with shear modulus of about $G = 0.387\,\mathrm{GPa}$ is an appropriate material for this biomeachnical application.

In order to prevent a technical collapse, the maximum tolerable torque τ_{max} is approximated by considering the yield strength σ_{per} of the applied material resulting in

$$\tau_{max} = \frac{\sigma_{per}\,I_t}{R} \ . \tag{10}$$

By inserting the maximum torque τ_{max} into (3), the maximum resulting deflection ϑ_{max} can be calculated.

V. SIMULATIVE EVALUATION

The enhanced efficiency of compliant actuator concepts is a relevant improvement for an biomechanical application in mobile robotics or prosthetic devices. In 2009, Vanderborght et al. compared the energy consumption of different adaptable, compliant actuator designs based on a simulation of a pendulum motion. The applied pendulum had a single degree of freedom and was modeled in reference to the leg of the biped robot, named Lucy [29]. In order to focus

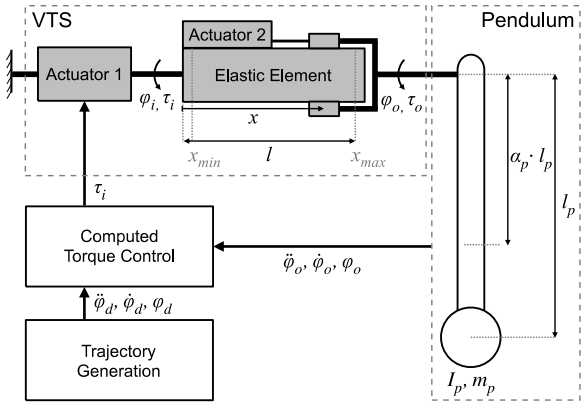

Fig. 4. Block diagram of mechanical setup and control architecture.

on the performance of the elastic concepts, all actuators were assumed to operate under ideal working conditions. In addition, no energy is consumed when a force is applied at a fixed position and no energy can be recovered. Neglecting the moment of inertia, the desired position is reached instantaneously [3]. The simulative evaluation of VTS is aligned to these studies by choosing the same mechanical setup and control architecture. This ensures best comparability of results and allows to assess VTS with regard to existing compliant actuator designs. In the evaluation, the power consumption of an ideal stiff actuator is used as a reference level.

The single degree of freedom pendulum consists of a rod with the inertia I_p and the length l_p as well as an attached point mass m_p. The center of gravity along the length l_p is specified by the factor α_p. Since the pendulum is driven by VTS directly, the actual angular position equals the angular output position φ_o. Based on the considerations in Section IV, the material of the elastic element is supposed to be polyethylene. The required input torque τ_i is calculated using computed torque control. The desired angular trajectory φ_s produced by a trajectory generator is a sine wave with an amplitude of $10\,^\circ$. Figure 4 illustrates the applied mechanical setup and control architecture. The mechanical parameters used in the simulation are listed in Table I.

The dynamic equation of the pendulum is given by

$$I_{rp}\,\ddot{\varphi_o} + m_p\,g\,\alpha\,l_p\,\sin(\varphi_o) = \tau_t\ , \tag{11}$$

where the moment of inertia with respect to the rotational axis results from $I_{rp} = m_p\,(\alpha_p\,l_p)^2 + I_p$. The torque τ_t is generated by the torsion of the elastic element. By applying a spring-damper model with the deflection ϑ, (4) is extended to

$$\begin{aligned}\tau_t &= k_{vts}\,\vartheta + c_{vts}\,\dot{\vartheta}\ ,\\ &= k_{vts}\,(\varphi_i - \varphi_o) + c_{vts}\,(\dot{\varphi}_i - \dot{\varphi}_o)\ .\end{aligned} \tag{12}$$

The damping constant c_{vts} is assumed to be proportional to the active length x and is approximated by the linear relation $c_{vts} = c_{rel}\,x$. The applied computed torque control combines a feedforward and feedback control to form a nonlinear control law which leads to a linearized closed-loop system. The effects of inertia, gravity as well as friction are compensated [31]. With (11) and (12), the equation of the computed torque control can be determined by

$$\begin{aligned}\tau_i &= k_{vts}\,\varphi_i + c_{vts}\,\dot{\varphi}_i\\ &= C_e\,\dot{\varphi}_o + G_e\\ &+ D_e\left[\ddot{\varphi}_s + k_p\,(\varphi_s - \varphi_o) + k_i\int(\varphi_s - \varphi_o)\,dt\right.\\ &\left.+\ k_d\,(\dot{\varphi}_s - \dot{\varphi}_o)\right]\end{aligned} \tag{13}$$

where the parameters C_e, G_e and D_e are specified by

$$C_e = 0\ , \tag{14}$$

$$G_e = m_p\,g\,\alpha_p\,l_p\,\sin(\varphi_o) + k_{vts}\,\varphi_0 + c_{vts}\,\dot{\varphi}_o\ , \tag{15}$$

$$D_e = I_{rp}\ . \tag{16}$$

The control parameters used in the simulation are listed in Table I.

For the survey of the average power consumption, the energy consumption of VTS is measured over a time period of 5 oscillation periods and is divided by the elapsed time span t_m. The total energy consumption can be partitioned into the motion energy that is applied for the pendulum motion E_m and the setting energy that is required to adjust the stiffness. The motion energy E_m depends on the current torsional torque τ_t and angular input velocity $\dot{\varphi}_i$ and is given by

$$E_m = \int_{t_m} |\tau_t\ \dot{\varphi}_i|\,dt\ . \tag{17}$$

The setting energy E_s is necessary to overcome the friction force while moving the counter bearing as stated in Section III. During the adjustment of the stiffness, which is presumed to happen instantaneously, the torsional torque τ_t

TABLE I
PARAMETERS OF MECHANICAL SETUP AND CONTROL [29], [30].

	Parameter	Value	Unit
VTS	G_{vts}	$3.87 \cdot 10^8$	Pa
	r_{vts}	$4.5 \cdot 10^{-3}$	m
	R_{vts}	$9.0 \cdot 10^{-3}$	m
	μ_{vts}	0.1	
	x_{min}	$10.0 \cdot 10^{-3}$	m
	x_{max}	$100.0 \cdot 10^{-3}$	m
	c_{rel}	0	$N\ s\ rad^{-1}$
	σ_{per}	30	$N\ mm^{-2}$
Pendulum	m_p	6.81	kg
	I_p	$11.05 \cdot 10^{-2}$	$kg\ m^2$
	l_p	0.45	m
	α_p	0.77	
	g	9.81	$m\ s^{-2}$
Control	k_p	8000.0	$Nm\ rad^{-1}$
	k_i	1600.0	$Nm\ rad^{-1}\ s^{-1}$
	k_d	50.0	$Nm\ s\ rad^{-1}$

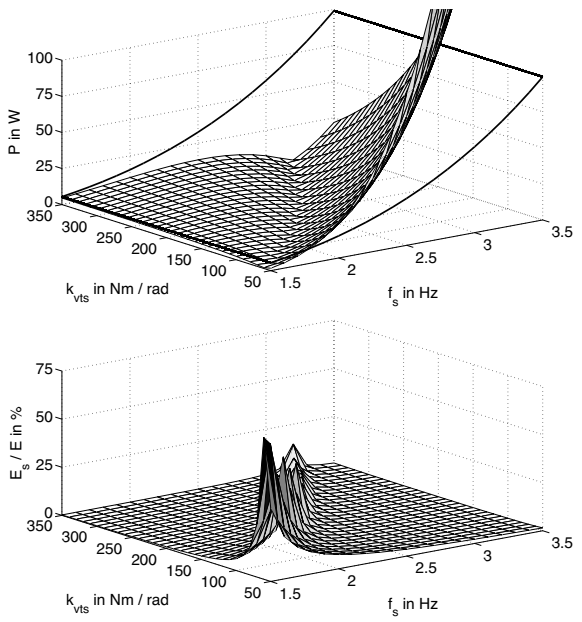

Fig. 5. *Top:* Power consumption P of VTS (shaded mesh) and an ideal stiff actuator (black line) versus frequency f_s and stiffness k_{vts}.
Bottom: Ratio between setting energy E_s and total energy consumption E versus frequency f_s and stiffness k_{vts}.

is required to be constant to ensure a steady angular output position φ_o. With these assumptions, the setting energy E_s is defined by

$$E_s = \int_{x_1}^{x_2} |F_f| \, dx \, , \\ = \left| \mu \frac{\tau_t}{R} \left(x_2 - x_1 \right) \right| \, . \tag{18}$$

The radial distance of the counter bearing r_n is assumed to equal to the outer radius R and the elastic element is supposed to have a neglectable damping constant c_{vts}. The average power consumption P results from the total energy consumption $E = E_m + E_s$ divided by the elapsed time t_m.

The simulation is performed in an iterative modality. Each simulation step provides a settle time of 20 oscillation periods followed by the measurement time of 5 oscillation periods. The frequency f_s is kept constant, while the stiffness k_{vts} is increased by a single step of $10\,\mathrm{Nm\ rad^{-1}}$ during settle time. The stiffness is adjusted at a phase of $\frac{\pi}{2}$ resulting in the maximum setting energy E_s, since the torsional torque τ_t peaks at this point. Figure 5 shows the power consumption of VTS over a stiffness range from $50\,\frac{\mathrm{Nm}}{\mathrm{rad}}$ to $350\,\frac{\mathrm{Nm}}{\mathrm{rad}}$ and a frequency range from 1.5 Hz to 3.5 Hz. The power consumption of an ideal stiff actuator is indicated by a black line on the axes planes.

Figure 5 presents the results of the simulative evaluation. The upper diagram shows that there is an optimal stiffness for each frequency resulting in a path of minimal power consumption in parameter space. For these stiffness values the frequency of the desired trajectory lies on to the current natural frequency of the controlled overall system. Compared to the ideal stiff actuator, the VTS concept provides lower average power consumption excluding the area of low stiffness and high frequency values. For low stiffness values, the deflection of the elastic element reaches high values in order to achieve a high output torque. In combination with high frequencies, this demands high deflection velocities, and thus has a negative effect on the average power consumption. Since there is an optimal stiffness for each desired frequency, an appropriate stiffness control strategy allows to avoid adverse combinations of frequency and stiffness values. The lower diagram illustrates the marginal impact of the setting energy E_s on the total energy consumption E beyond the path of minimal power consumption. Because of the comparatively low total energy consumption E within the power minimal area, the ratio of the setting energy E_s reaches up to 73.6 %, although its maximum value does not exceed 2.2 J.

As given by (10), the maximum accapteble torque τ_{max} of the applied hollow cylinder is specified by the yield strength σ_{per} of polyethylene. With the parameters given in Table I, the here proposed VTS configuration is able to provide an output torque τ_o of up to 32.2 Nm and a maximum deflection ϑ of 0.67 rad. The resulting output torque in simulation reaches high values for high frequencies. In combination with low stiffness values this leads to high deflections of the elastic element. Hence, the acceptable value is exceeded in these edge regions in both cases. To solve this problem, the application of glass fibre reinforced plastics with optimized fiber angle is suggested.

VI. CONCLUSIONS AND FUTURE WORKS

As mentioned in Section I and determined in Section IV, the VTS concept provides the possibility to develop compact and customizable actuator concepts with adjustable compliance. Thus, it is well-suited for the implementation in biomechanical or robotic applications with limited installation space. Based on the simple analytical models derived in Section III, the control of the stiffness adjustment and the whole VTS actuator can be implemented with reasonable effort. For this reason, a customization of VTS to the application can be conducted in software - e.g., an individualized stiffness characteristic. Additionally, a fundamental customization on hardware level as proposed in Section II is possible by changing the mechanics of the system - e.g., by material exchange or geometric modification.

Due to the results of the simulative evaluation in Section V, an optimal stiffness regarding power consumption exists for every trajectory. Hence, VTS should be operated at this optimum by means of an appropriate control strategy. In order to transmit higher torques at high deflections, while retaining the stiffness bandwidth, the usage of glass fiber reinforced plastics should be investigated. To optimize the loadability of the elastic element, the fiber angle should be examined and aligned to the loading condition.

Considering the average power consumption, the comparison of VTS to other contemporary approaches providing ad-

justable stiffness shows that it has comparable behaviour [3]. In the area of high frequency and low stiffness values, the MACCEPA concept from Vrije Universiteit Brussel provides lower average power consumption compared to all other concepts including VTS. Yet, operation in this area can be avoided by an appropriate stiffness control strategy. Two advantages of the VTS concept in comparison to the mechanically controlled concepts investigated in [3], are the low power consumption for setting and holding a desired stiffness and the ability to retain the chosen stiffness without readjustment during operation. Although the latest MACCEPA design provides a self-locking worm gear drive [32], readjustments are necessary, if changes in the kinematic alignment appear, and thus additional power is required to retain stiffness during motion.

In their future works, the authors will focus on implementing the VTS concept in biomechanical applications, as the concept complies to the requirements of an active prosthetic knee joint. Aiming on this, integrated design implementations - e.g., by placing actuator 1 inside the elastic element - and a prototype will be elaborated. Based on the prototype, experiments will be conducted in parallel to further simulative evaluation. With the results from these studies, the system and control design as well as the potential for energy storage will be optimized.

REFERENCES

[1] G. A. Pratt and M. M. Williamson, "Series elastic actuators," in *Proceedings of the 1995 IEEE/RSJ International Conference on Intelligent Robots and Systems*, 1995.

[2] S. Klug, T. Lens, O. von Stryk, B. Möhl, and A. Karguth, "Biologically inspired robot manipulator for new applications in automation engineering," in *Proc. of Robotik 2008*, 2008.

[3] B. Vanderborght, R. Van Ham, D. Lefeber, T. G. Sugar, and K. W. Hollander, "Comparison of Mechanical Design and Energy Consumption of Adaptable, Passive-compliant Actuators," *The International Journal of Robotics Research*, vol. 28, pp. 90–103, 2009.

[4] M. M. Williamson, "Series elastic actuators," Master Thesis, Massachusetts Institute of Technology, 1995. [Online]. Available: http://mit.dspace.org/handle/1721.1/6776

[5] T. Morita and S. Sugano, "Design and development of a new robot joint using a mechanical impedance adjuster," in *1995 IEEE International Conference on Robotics and Automation*, 1995.

[6] R. Van Ham, T. G. Sugar, B. Vanderborght, K. W. Hollander, and D. Lefeber, "Compliant Actuator Designs Review of Actuators with Passive Adjustable Compliance/Controllable Stiffness for Robotic Applications," *IEEE Robotics & Automation Magazine*, vol. 16, pp. 81–94, 2009.

[7] K. W. Hollander, R. Ilg, T. G. Sugar, and D. Herring, "An efficient robotic tendon for gait assistance," *Journal of Biomechanical Engineering*, vol. 128, pp. 788 – 791, 2006.

[8] J. Choi, S. Hong, W. Lee, S. Kang, and M. Kim, "A robot joint with variable stiffness using leaf springs," *IEEE Transactions on Robotics*, vol. 27, pp. 229–238, 2011.

[9] K. W. Hollander, T. G. Sugar, and D. Herring, "Adjustable robotic tendon using a 'jack spring'™," *Proceedings of the 2005 IEEE 9th International Conference on Rehabilitation Robotics*, pp. 113 – 118, 2005.

[10] B. Vanderborght, N. G. Tsagarakis, R. Ham, I. Thorson, and D. G. Caldwell, "MACCEPA 2.0: compliant actuator used for energy efficient hopping robot Chobino1D," *Autonomous Robots*, vol. 31, pp. 55–65, 2011.

[11] G. Tonietti, R. Schiavi, and A. Bicchi, "Design and control of a variable stiffness actuator for safe and fast physical Human/Robot interaction," *Proceedings of the 2005 IEEE International Conference on Robotics and Automation*, vol. 1, pp. 526–531, 2005.

[12] R. Schiavi, G. Grioli, S. Sen, and A. Bicchi, "VSA-II: a novel prototype of variable stiffness actuator for safe and performing robots interacting with humans," in *2008 IEEE International Conference on Robotics and Automation*, 2008.

[13] S. Wolf and G. Hirzinger, "A new variable stiffness design: Matching requirements of the next robot generation," in *2008 IEEE International Conference on Robotics and Automation*, 2008.

[14] J. Song and B. Kim, "Three types of dual actuator units for variable impedance actuation," Intelligent Robotics Laboratory, Dep. Of Mechanical Engineering, Korea University, 2010.

[15] A. Jafari, N. G. Tsagarakis, B. Vanderborght, and D. G. Caldwell, "A novel actuator with adjustable stiffness (AwAS)," in *2010 IEEE/RSJ International Conference on Intelligent Robots and Systems*, 2010.

[16] A. Jafari, N. G. Tsagarakis, and D. G. Caldwell, "AwAS-II: a new actuator with adjustable stiffness based on the novel principle of adaptable pivot point and variable lever ratio," in *2011 IEEE International Conference on Robotics and Automation*, 2011.

[17] J. S. Sulzer, M. A. Peshkin, and J. L. Patton, "MARIONET: an exotendon-driven rotary series elastic actuator for exerting joint torque," in *9th International Conference on Rehabilitation Robotics*, 2005.

[18] A. H. Stienen, E. E. Hekman, H. ter Braak, A. M. Aalsma, F. C. van der Helm, and H. van der Kooij, "Design of a rotational hydroelastic actuator for an active upper-extremity rehabilitation exoskeleton," in *2nd IEEE RAS & EMBS International Conference on Biomedical Robotics and Biomechatronics*, 2008.

[19] T. Umedachi and A. Ishiguro, "A development of a fully self-contained real-time tunable spring," in *2006 IEEE/RSJ International Conference on Intelligent Robots and Systems*, 2006.

[20] B. Verrelst, F. Daerden, D. Lefeber, R. Van Ham, and T. Fabri, "Introducing pleated pneumatic artificial muscles for the actuation of legged robots : a one-dimensional set-up," *Proceedings of the IEEE International Conference on Biomedical Robotics and Biomechatronics*, pp. 583 – 590, 2010.

[21] J. W. Hurst, J. E. Chestnutt, and A. A. Rizzi, "An actuator with physically variable stiffness for highly dynamic legged locomotion," in *2004 IEEE International Conference on Robotics and Automation*, 2004.

[22] I. Thorson, M. Svinin, S. Hosoe, F. Asano, and K. Taji, "Design considerations for a variable stiffness actuator in a robot that walks and runs," pp. 1–4, 2007.

[23] S. A. Migliore, E. A. Brown, and S. P. DeWeerth, "Biologically inspired joint stiffness control," in *Proceedings of the 2005 IEEE International Conference on Robotics and Automation*, 2005.

[24] O. Eiberger, S. Haddadin, M. Weis, A. Albu-Schäffer, and G. Hirzinger, "On joint design with intrinsic variable compliance: derivation of the DLR QA-Joint," in *2010 IEEE International Conference on Robotics and Automation*, 2010.

[25] K. Koganezawa, Y. Shimizu, H. Inomata, and T. Nakazawa, "Actuator with non linear elastic system (ANLES) for controlling joint stiffness on antaonistic driving," in *2004 IEEE International Conference on Robotics and Biomimetics*, 2004.

[26] J. Choi, S. Park, W. Lee, and S. Kang, "Design of a robot joint with variable stiffness," in *IEEE International Conference on Robotics and Automation, 2008.*, 2008.

[27] B. Vanderborght, N. G. Tsagarakis, C. Semini, R. Van Ham, and D. G. Caldwell, "MACCEPA 2.0: Adjustable compliant actuator with stiffening characteristic for energy efficient hopping," *Proceedings of the IEEE International Conference on Robotics and Automation*, pp. 544–549, 2009.

[28] D. Gross, W. Hauger, J. Schröder, and W. A. Wall, *Technische Mechanik 2: Elastostatik*. Springer, 2012, ch. 5.

[29] B. Vanderborght, B. Verrelst, R. V. Ham, M. V. Damma, P. Beyl, and D. Lefeber, "Development of a compliance controller to reduce energy consumption for bipedal robots," *IEEE Robotics & Automation Magazine*, 2009.

[30] H. Beerbaum, "Ermittlung strukturbezogener bruchmechanischer Werkstoffkenngrößen an Polyethylen-Werkstoffen," Ph.D. dissertation, Martin-Luther-Universität, Halle-Wittenberg, 1999.

[31] R. Kelly, V. S. Davila, and J. A. L. Perez, *Control of Robot Manipulators in Joint Space*. Springer, 2005.

[32] "MACCEPA datasheet," 2011. [Online]. Available: www.viactors.eu